# Kinetic Monte Carlo simulations of optimization of self-assembly quantum rings growth strategy based on substrate engineering*

Liu Jian-Tao(刘建涛), Feng Hao(冯 昊), Yu Zhong-Yuan(俞重远)†, Liu Yu-Min(刘玉敏), Shi Qiang(石 强), Song Xin(宋 鑫), Zhang Wen(张 文), and Peng Yi-Wei(彭益炜)

*State Key Laboratory of Information Photonics and Optical Communications (Beijing University of Posts and Telecommunications), Beijing* 100876, *China*

(Received 14 July 2012; revised manuscript received 13 October 2012)

In this paper, the kinetic Monte Carlo simulations of the self-assembly quantum rings (QRs) based on the substrate engineering, which is related to the eventual shape of the formed quantum ring, are implemented. According to the simulation results, the availability of the QR with tunable size and the formation of smooth shape on the ideal flat substrate are checked. Through designing the substrate engineering, i.e., changing the depth, the separation and the ratio between the radius and the height of the embedded inclusions, the position and size of QR can be controlled and eventually the growth strategy of optimizing the self-assembly QRs is accomplished.

**Keywords:** quantum rings, kinetic Monte Carlo, self-assembly, substrate engineering

**PACS:** 68.55.ag, 81.10.Aj, 81.16.Dn **DOI:** 10.1088/1674-1056/22/4/046801

## 1. Introduction

Recently, due to the unique optical and electronic properties, self-assembly quantum rings (QRs)[1,2] have been intensively studied to develop the potential applications in optoelectronics and semiconductor devices. Moreover, QRs also offer a crucial opportunity to investigate the unusual magnetic behavior of susceptibility and the Aharonov–Bohm effect.[3–5] Considering the great contribution to the functional units in fabricating electronic, optoelectronic, and magnetic storage devices with nanoscale dimensions, there are still challenges relating to QRs.[6]

With the development of science and technology, advanced growth techniques have made it possible to form a variety of nanostructures.[7] Since the first example of self-assembly InAs/GaAs ring-shaped quantum dots (QDs) was reported in 1997, outstanding contributions have been made to this novel structure. In order to attain QRs with different dimensions and shapes, a lot of fabrication methods of semiconductor QRs have therefore emerged in the past years. The traditional lithographic technique has been used to fabricate QRs.[8,9] However, to the best of our knowledge, there is little research about the popular fabrication of small rings. Although the droplet epitaxy[10,11] has been intensively investigated as an important self-assembly technique for semiconductor QRs in the lattice-matched systems such as GaAs/AlGaAs and the lattice-mismatched systems such as InGaAs/GaAs, positions of QRs are uncontrollable and the regular array of QRs seems to be hardly achieved due to the irregular distribution of droplets on substrates.

A method based on the substrate engineering is suggested as a candidate for self-assembly QRs. In order to accomplish the self-assembly process of the QRs based on the lattice-mismatched system, people provide many kinds of methods by changing the structure of the substrate.[12–16] It proves that the way of embedding the QDs in the substrate could be used to fabricate QRs. Self-organization technology with a cap layer is suitable for the lattice mismatched system. It could produce QRs with tunable size, smooth shape, and regular array, which are highly desired.

In this paper, by the kinetic Monte Carlo method, self-assembly QRs with different growth parameters are simulated. The self-assembly QRs are related to the final shape of the formed QRs. Furthermore, we accomplish the kinetic Monte Carlo simulations to check the availability of the QRs with tunable size and the formation of smooth shape on the ideal flat substrate.[17] Both the separation distance and the ratio between the radius and height of the embedded inclusions prove indispensable to form the ideal QRs in the KMC simulations. Eventually, we obtain the growth strategy of optimizing self-assembly QRs by designing the substrate engineering.

The reminder of this paper is organized as follows. We briefly introduce strain distribution theory of the substrate induced by the embedded inclusions in Section 2. In Section 3, we provide the theory of kinetic Monte Carlo simulation method. Our simulation and analysis results of the performance of the scheme are outlined in Section 4. Finally the conclusions are drawn in Section 5.

*Project supported by the National Natural Science Foundation of China (Grant Nos. 60908028 and 60971068), the Program for New Century Excellent Talents in University, China (Grant No. NTCE-10-0261), and the Chinese Universities Science Fund (Grant No. 2011RC0402).

†Corresponding author. E-mail: yuzhongyuan30@gmail.com

© 2013 Chinese Physical Society and IOP Publishing Ltd 

## 2. Strain distributions theory

In order to execute the KMC simulations we first should know the strain distribution which could be calculated by the finite element method and continuous elastic theory on the substrate. Briefly, the dependence of strain component on stress component can be set up by using a stiffness matrix $\boldsymbol{D}$, and then the strain and the stress[18] may be expressed as two column vectors,[19]

$$\varepsilon = \begin{bmatrix} \varepsilon_{xx} \\ \varepsilon_{yy} \\ \varepsilon_{zz} \\ \varepsilon_{xy} \\ \varepsilon_{yz} \\ \varepsilon_{zx} \end{bmatrix} = \begin{bmatrix} \partial u/\partial x \\ \partial v/\partial y \\ \partial w/\partial z \\ (\partial u/\partial y + \partial v/\partial x)/2 \\ (\partial v/\partial z + \partial w/\partial y)/2 \\ (\partial u/\partial z + \partial w/\partial x)/2 \end{bmatrix} \tag{1}$$

and

$$\boldsymbol{\sigma} = \begin{bmatrix} \sigma_{xx} \\ \sigma_{yy} \\ \sigma_{zz} \\ \sigma_{xy} \\ \sigma_{yz} \\ \sigma_{zx} \end{bmatrix} = \boldsymbol{D}(\varepsilon - \varepsilon_0) + \sigma_0, \tag{2}$$

where $u$, $v$, and $w$ are the displacements along the coordinates $x$, $y$, and $z$ directions respectively. For the cubic crystal the $\boldsymbol{D}$ matrix can be expressed as

$$\boldsymbol{D} = \begin{bmatrix} C_{11} & C_{12} & C_{13} & 0 & 0 & 0 \\ C_{12} & C_{11} & C_{13} & 0 & 0 & 0 \\ C_{13} & C_{13} & C_{33} & 0 & 0 & 0 \\ 0 & 0 & 0 & (C_{11}-C_{12})/2 & 0 & 0 \\ 0 & 0 & 0 & 0 & C_{44} & 0 \\ 0 & 0 & 0 & 0 & 0 & C_{44} \end{bmatrix}. \tag{3}$$

As can be seen, there exist three independent elastic constants. The lattice constants in the QD system vary with coordinate, therefore the elastic energy can be expressed as an integral equation,

$$U = \frac{1}{2}\int C_{ijkl}\left(\varepsilon_{ij} - \varepsilon^0_{ij}\delta_{ij}\right)\left(\varepsilon_{kl} - \varepsilon^0_{kl}\delta_{kl}\right) \mathrm{d}v, \tag{4}$$

where $\varepsilon^0_{ij}$ are the components of initial strain in the QD system. In a QD region, the initial strain is the lattice mismatch of the heterostructure material. In the surrounding barriers, the initial strain is zero. The lattice mismatch can be expressed as

$$\varepsilon^0_{i,j} = \begin{cases} \varepsilon^0_{xx} = \varepsilon^0_{yy} = \dfrac{a_{\mathrm{dot}} - a_{\mathrm{sub}}}{a_{\mathrm{sub}}}, \\ \varepsilon^0_{zz} = \dfrac{c_{\mathrm{dot}} - c_{\mathrm{sub}}}{c_{\mathrm{sub}}}, \\ \varepsilon^0_{i,j} = 0, \quad i \neq j, \end{cases} \tag{5}$$

substituting Eqs. (1), (2), and (5) into Eq. (4), the elastic strain energy of the QD system can be expressed as

$$\begin{aligned} U = \frac{1}{2}\iiint \{ & C_{11}\left(\varepsilon^2_{xx} + \varepsilon^2_{yy}\right) + C_{33}\varepsilon^2_{zz} \\ & + 2C_{12}\varepsilon_{xx}\varepsilon_{yy} + 2C_{13}\varepsilon_{zz}\left(\varepsilon_{xx} + \varepsilon_{yy}\right) \\ & + 4C_{44}\left(\varepsilon^2_{yz} + \varepsilon^2_{xz}\right) + 2\left(C_{11} - C_{12}\right)\varepsilon^2_{xy} \\ & - 2\varepsilon^2_{xx}\left(C_{11} + C_{12}\right)\left(\varepsilon_{xx} + \varepsilon_{yy}\right) - 2C_{33}\varepsilon_{zz}\varepsilon^0_{zz} \\ & - 2C_{13}\left[2\varepsilon_{zz}\varepsilon^0_{xx} + \varepsilon^0_{zz}\left(\varepsilon_{xx} + \varepsilon_{yy}\right)\right] \\ & + 2C_{11}\left(\varepsilon^0_{xx}\right)^2 + C_{33}\left(\varepsilon^0_{zz}\right)^2 \\ & + 2\varepsilon^0_{xx}\left(C_{12}\varepsilon^0_{xx} + 2C_{13}\varepsilon^0_{zz}\right)\} \mathrm{d}v. \end{aligned} \tag{6}$$

## 3. Kinetic Monte Carlo simulations

In order to check the reliability of the proposed technique, we perform the KMC simulations. In our imitation process, the deposition of the third material atoms and the diffusion of the atoms on the substrate are included. Starting with a perfect, defect free, wetting layer, which is not simulated explicitly, we deposit adatoms randomly with a given flux rate and probability distribution of a random number is uniform distribution. The models are based on a two-dimensional (2D) solid-on-solid model [20,21] of epitaxial growth, presented by Zhu *et al.*[22] and Lam *et al.*[23] under the assumption of a simple cubic lattice structure with neither vacancies nor overhangs. Our model is developed from previous work.[24] In order to account for the adsorption and desorption motion of atoms, an up-down ratio is also introduced. As is well known, the atom in the same plane moves toward a direction in a random manner, and the probability of the moving toward every direction is equivalent. The atoms on the substrate can still diffuse after the nucleation unless their neighboring positions are all occupied by other atoms. The hopping rate of a topmost atom follows the Arrhenius's law:[25]

$$p = \nu_0 \exp\left(-\frac{E_{\mathrm{S}} + E_{\mathrm{N}} + E_{\mathrm{sw}} - \Delta E}{\kappa_{\mathrm{B}} T}\right), \tag{7}$$

where $\Delta E$ is the strain energy, $k_{\mathrm{B}}T$ the thermal energy, $k_{\mathrm{B}}$ the Boltzmann constant, $\nu_0$ the attempt frequency, $E_{\mathrm{S}}$ and $E_{\mathrm{N}}$ are the binding energy to the surface and the neighboring atoms, respectively. In order to explain the motion of the atoms, an additional parameter Schwöbel step-edge barrier term $E_{\mathrm{SW}}$ is introduced. In most of the previous investigations just the neighboring atoms in the same high plane were taken into account. However, the neighboring atoms in the up layer and the down layer should be considered in the three-dimensional (3D) simulation. So, in our work, we take into account the interaction between the neighboring atoms in different planes.

We know that there are three kinds of bondings between two different atoms as shown in Fig. 1. As the result of the disparate bonding mode, the bonding energies are diverse between the two atoms, and they can be expressed by $E_{AA}$, $E_{AB}$, and $E_{BB}$. Figure 2 illustrates all the atoms diffusion processes considered in our simulations, showing an adatom moving on the flat terrace, stepping down at a step edge and detached

from a step edge. The activation barrier of the diffusion process is determined by the local bonding of the initial configuration and the interatomic bond energy. For the adatom terrace diffusion, the activation barrier is given by the bond energy of the adatom to its neighbor underneath. The activation barrier for the adatom stepping down is the terrace diffusion barrier plus an additional Schwöbel step-edge barrier. Similarly, the activation barrier for the adatom detached from a step edge is the terrace diffusion barrier plus the bond energy of the adatom to the neighboring atom at the step edge. Figure 3 shows the atom picture of the QR simulations, while the relevant parameters used in the simulations process are listed in Table 1. In the simulations, the three two-component situations mentioned above are taken into account. It should be noted that dealing with effective atoms hopping on a square lattice and the usage of effective energies should be understood as a mean-field approach. Implicit properties which lead to local fluctuations of the binding energies are taken into account. Such properties are, for example, the surface reconstruction and ratio change, which might occur in both time and space. As long as these fluctuations are small compared with the time scale of the fastest process modeled explicitly, there is no influence on the validity of our model. However, for convenience, we simplify the simulations by using the equation $E_{AA} = E_{AB} = E_{BB} = E_b$. We first set the strength of all single nearest bonds $E_b$ to be 0.2 eV, and reduce it by a factor of $\delta$ for the next nearest neighbors. To calculate diffusion barrier, the binding energy $E_{n,\text{initial}}$ at the initial site and the binding energy at the hop site $E_{n,\text{hop}}$ are respectively calculated by the following equations:

$$E_{\text{N}} = E_{n,\text{initial}} - gE_{n,\text{hop}}, \tag{8}$$

$$E_{n,\text{initial}} = mE_b + \delta nE_b, \tag{9}$$

$$E_{n,\text{hop}} = m'E_b + \delta n'E_b, \tag{10}$$

where $m(m')$ and $n(n')$ are the numbers of the nearest and the next nearest atoms around. Coupling constant $g = 0.3$ is used in the equation, which describes a weak coupling between the two adjacent lattice sites. We remark that due to the fact that the interaction between the substrate atoms and the depositing atoms decreases with atom height increasing, the binding energy of substrate atom to the surface $E_{\text{S}}$ exponentially decays with distance increasing, i.e.,

$$E_{\text{S}} = E_{\text{S0}} \exp\left(h_{\text{atom}}\right), \tag{11}$$

where $E_{\text{S0}}$ is set to be 1.35 eV, $h_{\text{atom}}$ is the height of the formed island. The material parameters in our simulations are the three species (Si, Ge, Sn), thus, we take the Ge/Si (001) system with embedded Sn inclusions for example to investigate the Ge QRs self-assembly. The lattice constants of Si, Sn, Ge are chosen to be 5.43, 6.489, 5.658 Å (1 Å = 0.1 nm), respectively. The relevant parameters used in the simulations are listed in Table 1.[26,27] Finally, to account for the up and down motion of the atoms, an additional factor $\mu$[25] is introduced, which is defined as the ratio between the probability for edge atoms to hop up and that for edge atoms to hop down. The factor $\mu$ should be larger than 1. Otherwise, all the atoms will tend to move into lower layers.

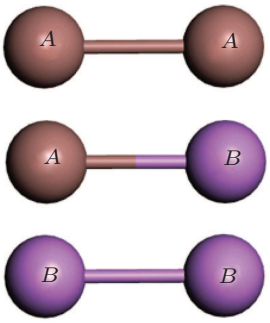



**Fig. 1.** (color online) Schematic plot of three kinds of bonding modes between two different atoms: (a) *AA*, (b) *AB*, (c) *BB*.

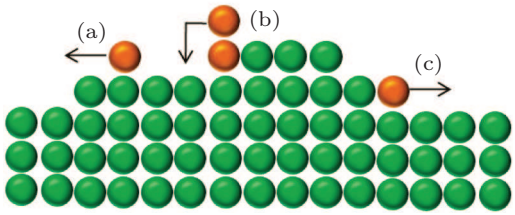



**Fig. 2.** (color online) Illustration of the diffusion processes considered in the simulation for the cases of (a) adatoms moving on the flat terrace, (b) stepping down at a step edge, (c) detached from a step edge.

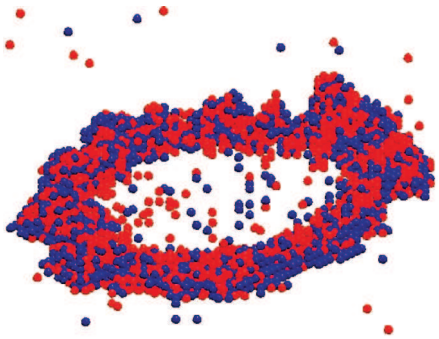


**Fig. 3.** (color online) Illustration of the 3D simulation picture of the quantum rings.

**Table 1.** Parameters of the KMC simulation.

| Temperature/K | Simulation area (lattice sites) | Flux/(ML/s) | Coverage |
|---|---|---|---|
| 818 | $200 \times 200$ | 1 | 0.15 |

## 4. Results and discussion

Two kinds of the models are built for our KMC simulation as shown in Fig. 4. One model as displayed in the Fig. 4(a), which shows how the finally formed QRs will transfer by changing the radius and the height of the single embedded inclusion. The other model as shown in Fig. 4(b) displays that with the radius and the height of the inclusions fixed, the

eventual resulting shapes of the QRs suffer a series of changes through changing the separation between the two embedded inclusions.

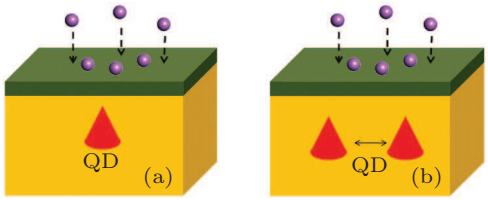



**Fig. 4.** (color online) (a) The model for the QR simulation by changing the radius-to-height ratio of the single embedded inclusion. (b) With the radius and the height of the embedded inclusions fixed, the model for the QR simulation through hanging the separation between the two neighbor embedded inclusions.

The diffusion behavior of an adatom on the wetting-layer surface is affected by surface chemical potential. The strain energy induced by embedding QD is the main factor to influence the distribution of the chemical potential which affects the diffusion barrier. In this case, we need to design and optimize the substrate structure to restrict the diffusion behaviors of surface atoms so as to acquire the expected structures. By investigating the diffusion behaviors of the surface atoms on different substrates, we can conclude that we obtain an approach to control the size and the shape to what we expect by changing the size of and the separation between the embedded inclusions through the KMC simulations.

Figure 5 reveals the radius-to-height ratio of the single embedded inclusion varying from 0.25 to 2.5, which leads to forming the different shapes of the QRs. Notice that the additional simulations are performed to confirm that the different ratios increased the width and the outer diameter of the QR, but the ring shape remains unchanged. Because the surface potential distribution of the growth surface is mainly affected by strain field, when the ratio is small, the extremum zone of surface strain field is more concentrated and bigger; moreover, the diffusion barrier causes atoms to nucleate in a narrow zone. With the increase of the ratio, the surface strain field (tensile strain) induced by embedded inclusion increases while the absolute value decreases. Therefore, the diffusion barrier of the growth surface reduces, which causes the atoms to be able to nucleate in a wider zone. Then, the outer ring diameter and the width of ring increase while the height of ring increases as shown in Fig. 6.

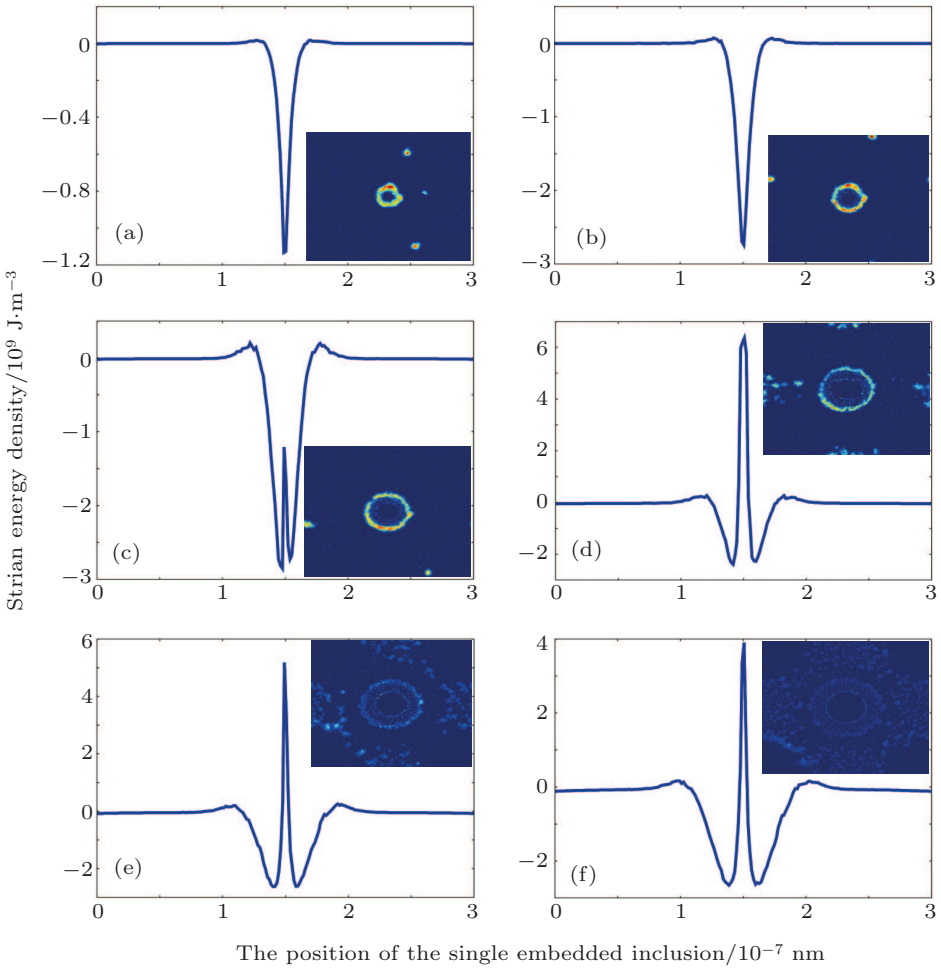



**Fig. 5.** (color online) QR shapes in the cases where radius-to-height ratios of the single embedded inclusion are (a) 0.25, (b) 0.5, (c) 1, (d) 1.5, (e) 2, (f) 2.5.

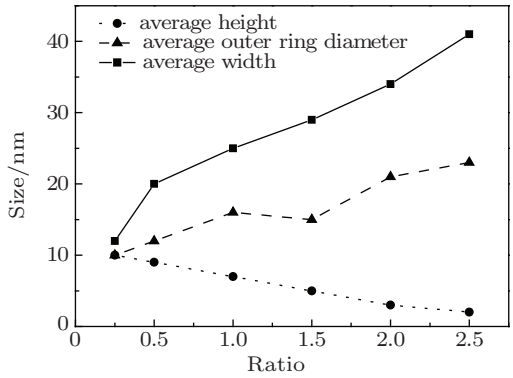



**Fig. 6.** (color online) Variation trends of the simulation results for the single embedded inclusion with radius-to-height ratio, with (i) the solid line showing the outer diameter of the formed QR, (ii) the dashed line representing the change of the width of the formed QR, and (iii) the dotted line referring to the height of the formed QR.

Furthermore, we study the influence of the separation between the nearest-neighboring inclusions on forming the QR. In order to realize the control of the QR dimension, we need to take the strain-coupling interaction between the two embedded inclusions into account. Similarly, when the separation is very small, the change of the potential well will have a large effect on the shape of the formed QR. We adopt two models (models A and B) to simulate how the shape changes by varying the separation from 0 nm to 60 nm. In model A the radius is 10 nm and the height is 20 nm while in model B, the radius is 20 nm and the height is 20 nm.

Figure 7 shows the transformation of model A. From the above discussion, we know that the distribution of the strain energy affects the atom diffusion behavior, which determines the final shape and size of the formed QR. From Fig.7, we can observe that the strain energy of the central position decreases with separation increasing. When the separation equals 60 nm, the absolute value of the strain energy of the central position is relatively small so that the interaction could be neglected. Now, the strain-coupling interaction between the embedded inclusions declines obviously, and the growth surface becomes two independent strain field distributions, which consequently result in two independent QRs. As shown in Fig. 7(d), we can survey that the formed QR shape turns oval-shaped instead, which is related to the change of the distance in the length direction. When the separation is 10 nm, it reaches a critical distance. After the critical separation, the shape of the formed QR deforms more and more seriously with the separation increasing.

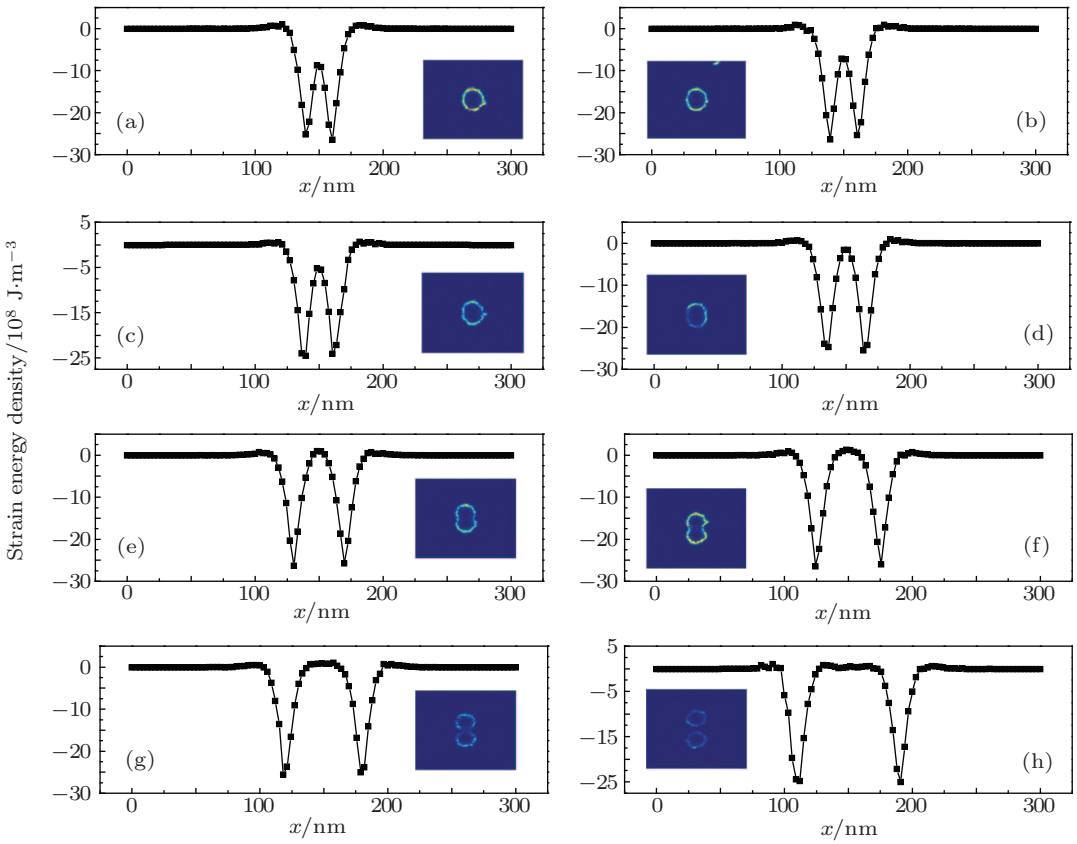



**Fig. 7.** (color online) The final shapes of the formed QRs from the simulation with the separation between the two embedded inclusions being: (a) 0 nm, (b) 2 nm, (c) 4 nm, (d) 10 nm, (e) 20 nm, (f) 30 nm, (g) 40 nm, and (h) 60 nm.

On the other hand, we also investigate the effect on the final shape of the QRs through changing the separation between the two nearest-neighboring embedded inclusions from 0 nm to 60 nm for model B which can be seen from Fig. 8. Due to the different dimensions between the two models, the strain distribution of model B is different from that of model A. Being similar to the circumstance of model A, the strain coupling interaction between the embedded inclusions are so strong that a maximum zone comes into being on the growth surface. With the increase of the separation distance, the strain field of the surface starts to be detached, and gradually produces two independent maximum zones which finally lead to the formation of two independent ORs. Compared with model A, the formed QRs of model B are of large size because of its wider maximum zone of strain field.

From the simulations in Fig. 8, it can be concluded that the bigger the radius-to-height ratio, the bigger the size of QRs is. When the separation is small, the large dimensional QRs could be carried out by designing the embedded inclusion project; when the separation is large, the double QRs and the QR molecules can be controlled through designing the substrate engineering.

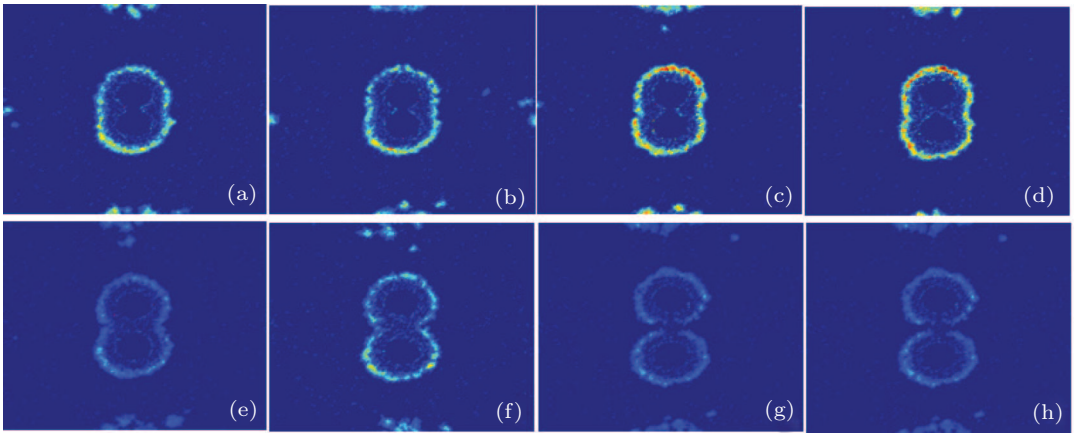



**Fig. 8.** (color online) The simulation results of model B with the separation between the two nearest-neighboring embedded inclusions being (a) 0 nm, (b) 2 nm, (c) 4 nm, (d) 10 nm, (e) 20 nm, (f) 30 nm, (g) 40 nm, (h) 60 nm.

In the Stranski–Krastanov growth mode, temperature and flux rate are also key factors influencing the quality of quantum ring growth. A special effort is made to examine the influence of the self-consistently calculated strain field. It should be noted that, however, the main interest of this work is not to present an optimized set of growth parameters. At the low temperature, because of the lack of adequate thermal activation energy, atoms that have been deposited on the substrate surface can not only diffuse into narrow area, but also overcome the binding energy to surface and neighboring atoms, and form QRs with big size and low height. With the increase of temperature, the thermal activation energy increases, and atoms can overcome binding energy to the up-layer. At the same time, flux rate also has an influence on atom density on the substrate in unit time and on the rate of nucleation as well. Furthermore, the influences of temperature and flux rate on quantum ring composition will be investigated in the next work.

## 5. Conclusions

We investigated the different shapes of the formed QRs by varying the separation between the two nearest-neighboring embedded inclusions through the KMC simulation. With separation changing, the KMC simulation results show that the formed QR varies from one to two independent rings. We also concluded that there will be a critical separation with the distance increasing, therefore, the final shape of the quantum ring will be covered at the central position. Then, it is obvious that we can have a method to control the size and shape of the formed QR which is what we expected, by varying the dimensions of and separation between the embedded inclusions. The kinetic Monte Carlo model we have used is effective and useful for studying the growth mode and atomic kinetics during the growth of the semiconductor QRs. Eventually, the final simulation results indicate that the controlling of the position and size of QR is available and the growth strategy of optimizing self-assembly QRs can be achieved by designing the substrate engineering.

## References

[1] Földi P, Kálmán O, Benedict M G and Peeters F M 2006 *Phys. Rev. B* **73** 155325
[2] Bayer M, Korkusinski M, Hawrylak P, Gutbrod T, Michel M and Forchel A 2003 *Phys. Rev. Lett.* **90** 186801
[3] Climente I J, Planelles J and Jaskólski W 2003 *Phys. Rev. B* **68** 075307
[4] Keyser U F, Fühner C, Borck S, Haug R J, Bichler M, Abstreiter G and Wegscheider W 2003 *Phys. Rev. Lett.* **90** 196601
[5] Li B and Peeters F M 2011 *Phys. Rev. B* **83** 115448
[6] Leon R, Petroff P M, Leonard D and Fafard S 1995 *Science* **267** 1966

[7] Klopf F, Reithmaier P and Forchel A 2000 *Appl. Phys. Lett.* **77** 1411
[8] Kiravittaya S, Rastelli A and Schmidt O G 2005 *Appl. Phys. Lett.* **87** 243112
[9] Lee J Y, Noordhoek M J, Smereka P, McKay H and Millunchick J M 2009 *Nanotechnology* **20** 285305
[10] Somaschini C, Bietti S, Koguchi N and Sanguinetti S 2011 *Nanotechnology* **22** 185602
[11] Somaschini C, Bietti S, Koguchi N, Sanguinetti S and Fedorov A 2010 *Nanotechnology* **21** 125601
[12] Atkinson P, Kiravittaya S, Benyoucef M, Rastelli A and Schmid O G 2008 *Appl. Phys. Lett.* **93** 101908
[13] Wang Z M, Liang B L, Sablon K A and Salamo G J 2006 *Appl. Phys. Lett.* **89** 043113
[14] Wang Z M, Liang B L, Sablon K A and Salamo G J 2007 *Appl. Phys. Lett.* **90** 113120
[15] Lin S Y, Tseng C C, Chung T H, Liao W H, Chen S H and Chyi J I 2010 *Nanotechnology* **21** 295304
[16] Polojärvi V, Schramm A, Guina M, Stemmann A and Heyn C 2011 *Nanotechnology* **22** 105603
[17] Tan X, Li X L and Yang G W 2008 *Phys. Rev. B* **77** 245322
[18] Liu Y M, Yu Z Y, Ren X M and Xu Z H 2008 *Chin. Phys. B* **17** 3471
[19] Liu Y M, Yu Z Y, Ren X M and Huang Y Z 2006 *Acta Phys. Sin.* **55** 5023 (in Chinese)
[20] Tan X, Ouyang G and Yang G W 2006 *Phys. Rev. B* **73** 195322
[21] Tan X, Ouyang G and Yang G W 2006 *Appl. Phys. Lett.* **88** 263116
[22] Zhu R, Pan E and Chung P W 2007 *Phys. Rev. B* **75** 205339
[23] Lam C H, Lung M T and Sander L M 2008 *J. Sci. Comput.* **37** 73
[24] Song Y X, Yu Z Y and Liu Y M 2008 *Acta Phys. Sin.* **57** 2399 (in Chinese)
[25] Brunev D V, Neizvestny I G, Shwartz N L and Yanovistkaja Z S 2001 *Nanotechnology* **12** 413
[26] Marchetti R, Montalenti F, Miglio L, Capellini G, Seta M D and Evangelisti F 2005 *Appl. Phys. Lett.* **87** 261919
[27] Seta M D, Capellini G and Evangelisti F 2005 *Phys. Rev. B* **71** 115308